ORIGINAL RESEARCH
published: 03 November 2021
doi: 10.3389/fcell.2021.738731

OPEN ACCESS

Edited by:
Zhao-Jia Ge,
Qingdao Agricultural University, China

Reviewed by:
Ashutosh Kumar,
All India Institute of Medical Sciences Patna, India
Bellamkonda K. Kishore,
University of Utah Health Care, United States

****Correspondence:***
António M. Galvão
antonio.galvao@babraham.ac.uk

Specialty section:
This article was submitted to Molecular and Cellular Reproduction, a section of the journal Frontiers in Cell and Developmental Biology

Received: *09 July 2021*
Accepted: *04 October 2021*
Published: *03 November 2021*

Citation:
Adamowski M, Wołodko K, Oliveira J, Castillo-Fernandez J,

INTRODUCTION

Obesity leads to chronic systemic inflammation, a process mostly promoted by the continuous expansion of adipose tissue (Hotamisligil and Erbay, 2008; Odegaard and Chawla, 2008). Importantly, obesity is strongly linked to reproductive failure and infertility in women (Chu et al., 2007). The ovaries of mice fed a high-fat diet (HFD) show increased apoptosis and fewer mature oocytes (Jungheim et al., 2010). Furthermore, we have recently identified a striking link between maternal body weight in diet-induced obese (DIO) mice and global gene expression in cumulus cells (Wołodko et al., 2020). Other readouts of ovarian failure during maternal obesity comprise lipotoxicity, endoplasmic reticulum (ER) stress, and mitochondrial dysfunction (Wu et al., 2010). Ultimately, impaired ovarian function in obese mothers determines poor oocyte quality and abnormal embryo

ob/ob, which are obese and lack leptin, denoting once more the important link between NLRP3 and leptin activity.

MATERIALS AND METHODS

Animals and Protocols

Breeding pairs were purchased from Jackson Laboratories (Bar Harbor, ME, United States). Female C57BL/6J (B6) mice (8-week old) and B6.Cg-Lepob/J (*ob/ob*) were housed in the Animal Facility of Institute of Animal Reproduction and Food Research, Polish Academy of Sciences in Olsztyn. Mice were housed with free access to food and water for the duration of the study (humidity 50 10%; 23

inhibitors (Pierce Phosphatase Inhibitor Mini Tablets 88667; Thermo Fisher Scientific) and incubating on ice for 1 h. After centrifugation (20,000 *g*, 15 min, 4 C), the supernatants were collected, and protein concentration was determined with the Smith et al. (1985) copper/bicinchoninic assay [Copper (II) Sulfate, C2284; Sigma and Bicinchoninic Acid Solution, B9643; Sigma Aldrich]. Samples were run (40 mg of protein) on 10–18% polyacrylamide gels. After transfer, the membranes were blocked in PBS solution containing 3% powdered milk for 1 h. Immunoblotting was performed using the primary antibodies NLRP3 (AG-20B-0014-C100; Adipogen), CASP1 (ab108362; Abcam), IL-18 (ab71495; Abcam), b-actin (A2228; Sigma Aldrich) and glyceraldehyde 3-phosphate dehydrogenase (GAPDH, ab9485; Abcam) on nitrocellulose (10600009; GE Healthcare Life Science) or polyvinylidene fluoride (PVDF) membrane (IPVH00010; Merck Millipore). Primary antibodies were incubated overnight at 4 C. The following day, proteins were detected by incubating the membranes with polyclonal anti-mouse horseradish peroxidase (HRP)-conjugated secondary (1:10,000, 31430; Thermo Fisher Scientific), polyclonal anti-rabbit HRP-conjugated secondary (1:20,000, 31460; Thermo Fisher Scientific), polyclonal anti-mouse alkaline phosphatase-conjugated secondary (1:10,000, 31321; Thermo Fisher Scientific), and polyclonal anti-rabbit alkaline phosphatase-conjugated secondary (1:10,000, A3687; Sigma Aldrich) antibodies, for 1.5 h in the chemiluminescence method or 2.5 h in the colorimetric method at RT. All antibody specifications are summarized in **Table 1**. Immunocomplexes were visualized subsequently using chemiluminescence detection reagent (SuperSignal West Femto kit, 34095; Thermo Fisher Scientific) or chromogenic substrate NBT/BCIP diluted 1:50 (11681451001; Roche) in alkaline phosphate buffer. Band density for each of the target protein was normalized against b-actin for NLRP3 and IL-18, while GAPDH was used for CASP1 as a reference protein. Finally, bands were quantified using the ChemiDoc or VersaDoc MP 4000 imaging system (Bio-Rad). Quantitative measurements of blot intensity were performed using ImageLab software.

TABLE 1 | Specification of antibodies used for Western blotting.

Antibody name and specificity	Company, Cat No., RRID No.	Antibody dilution
Mouse monoclonal against NLR family pyrin domain-containing 3 (NLRP3)	AdipoGen Cat# AG-20B-0014, RRID:AB_2490202	1:1,000
Rabbit monoclonal against caspase 1 (CASP1)	Abcam Cat# ab108362, RRID:AB_10858984	1:1,000
Rabbit polyclonal against interleukin-18 (IL-18)	Abcam Cat# ab71495, RRID:AB_1209302	1:250
Mouse monoclonal against b-actin	Sigma-Aldrich Cat# A2228, RRID:AB_476697	1:10,000
Rabbit polyclonal against glyceraldehyde 3-phosphate dehydrogenase (GAPDH)	Abcam Cat# ab9485, RRID:AB_307275	1:2,500
Goat anti-mouse IgG (HCL) secondary antibody, HRP	Thermo Fisher Scientific Cat# 31430, RRID:AB_228307	1:1,000
Goat anti-rabbit IgG (HCL) secondary antibody, HRP	Thermo Fisher Scientific Cat# 31460, RRID:AB_228341	1:20,000
Goat anti-mouse IgG (HCL) secondary antibody, AP	Thermo Fisher Scientific Cat# 31321, RRID:AB_10959407	1:1.000

Total RNA Isolation and cDNA Synthesis

Total RNA was extracted from whole ovary and 10 mg of liver, using TRI reagent (T9424; Sigma Aldrich) following the instructions of the manufacturer. RNA samples were stored at 80 C. Concentration and quality of RNA was determined spectrophotometrically, and the ratio of absorbance at 260 and 280 ($A_{260=280}$) was analyzed confirming good RNA quality. Subsequently, 2 mg of RNA was reverse transcribed into cDNA using Maxima First Strand cDNA Synthesis Kit for RT-qPCR (K1642; Thermo Fisher Scientific) (Galvão et al., 2012).

Real-Time PCR

Real-time PCR assays were performed in a 7900 Real-time System (Applied Biosystems), using a default thermocycler program for all genes: a 10-min preincubation at 95 C was followed by 45 cycles of 15 s at 95 C and 1 min at 60 C. A further dissociation step (15 s at 95 C, 15 s at 60 C, and 15 s at 95 C) ensured the presence of a single product. *Ribosomal protein L37 (Rpl37)* was chosen as a housekeeping gene and quantified in each real-time assay together with the target gene. Based on gene sequences in GenBank (National Center for Biotechnology Information), the primers for *Nlrp3*, *Casp1*, *Il-1*b, *Il-18*, *Asc*, *Il-10*, and *Tnf*, which sequences are presented in **Table 2**, were designed using Primer Express 3.0 software (Applied Biosystems). All reactions were carried out in duplicates in 384-well plate (4309849; Applied Biosystems) in 12 ml of total solution volume (Galvão et al., 2014). The data were analyzed using the real-time PCR Miner algorithm (Zhao and Fernald, 2005).

Enzyme-Linked Immunosorbent Assay Immunoassay

The concentrations of IL-1b in tissue extracts of ovaries and livers were determined using an IL-1 beta Pro-form Mouse Uncoated ELISA kit (88-8014-22; Thermo Fisher Scientific) following the instructions of the manufacturer.

TABLE 2 | Specific primers used for quantitative real-time PCR.

Gene name	Gene symbol	GenBank accession No.	Sequences 5′–3′	Length (base pairs)
NLR family pyrin domain-containing 3	*Nlrp3*	NM_145827.4	F: TGGATGGGTTTGCTGGGATA R: TGCTTGGATGCTCCTTGACC	190
Caspase 1	*Casp1*	NM_009807.2	F: CATGCCGTGGAGAGAAACAA R: GGTGTTGAAGAGCAGAAAGCAA	151
Interleukin-1b	*IL-1*b	NM_008361.4	F: TTGACGGACCCCAAAAGATG R: GCTTCTCCACAGCCACAATGA	144
Interleukin-18	*Il-18*	NM_008360.2	F: GAAGAAAATGGAGACCTGGAATCA R: TCTGGGGTTCACTGGCACTT	157
Apoptosis-associated speck-like protein-containing A CARD	*Asc*	NM_023258.4	F: GCTTAGAGACATGGGCTTACAGGA R: CCAGCACTCCGTCCACTTCT	179
Interleukin-10	*Il-10*	NM_010548.2	F: CCTGGGTGAGAAGCTGAAGAC R: CTGCTCCACTGCCTTGCTCT	91
Tumor necrosis factor	*Tnf*	NM_001278601.1	F: GCCACCACGCTCTTCTGTCT R: TGAGGGTCTGGGCCATAGAA	106
Ribosomal protein L37	*Rpl37*	NM_026069.3	F: CTGGTCGGATGAGGCACCTA R: AAGAACTGGATGCTGCGACA	108

Statistical Analysis and Data Presentation

Statistical analyses were performed using the GraphPad Prism Software (Version 9.01, GraphPad Software, Inc.; La Jolla, CA, United States). Sample normal distribution was determined using the D'Agostino–Pearson omnibus test. Mann–Whitney test, simple *t*-test, or multiple unpaired *t*-test were used to analyze the data, and statistical significance was calculated with Bonferroni–Sidak corrections for multiple comparison, depending on the experiment (details in figure legend). Results were presented as means with standard deviation. Differences between means for all tests were considered statistically significant if $p < 0.05$.

RESULTS

NOD-Like Receptor Protein 3 Inflammasome Components Expression Change in the Ovary of Cyclic Mice

We first sought to characterize the expression of NLRP3-induced inflammasome components in the ovaries of mice throughout the estrous cycle. Fifteen female 8-week-old C57BL/6 (B6) mice were treated with hormones in order to synchronize the estrous cycle (**Figure 1A**). Ovaries were collected in the E and D stage and further processed for mRNA or protein expression analysis, respectively. Real-time PCR analysis (n = 6–7/group) revealed increased levels of *Casp1*, *Il-1*b, and *Il-18* mRNA in the D stage (**Figure 1B**, $p < 0.05$). Moreover, Western blotting (n = 7–8/group) revealed increased NLRP3 protein expression in D (**Figure 1C**,

inflamm Tf 2.1l1[(<)]TJ/F201 9.5 Tf 12105 0 Td [(0.05,ed)-0((wa)1(s)-037(Iled)-0((wa)1(s)-035(t)-4(he)-039(p-p(Lepd(he)-03[(p24up)1

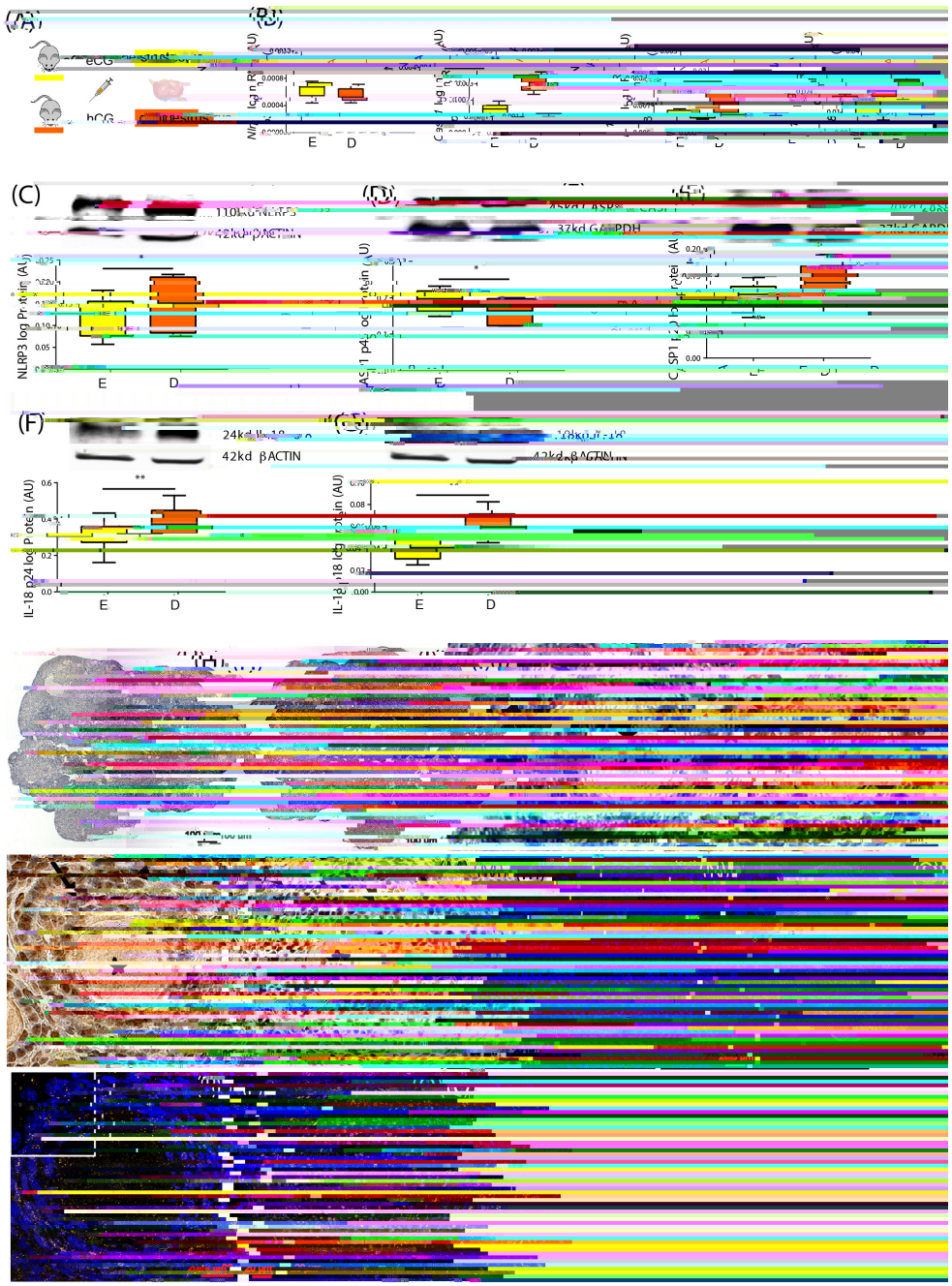

FIGURE 1 | Characterization of NOD-like receptor protein 3 (NLRP3) expression in the ovary of cyclic mice. **(A)** Experimental design: estrous cycle synchronization with equine chorionic gonadotropin (eCG) and human chorionic gonadotropin (hCG) as previously described (Hasegawa et al., 2016). Ovaries were collected from animals in the estrus **(E)** or diestrus **(D)** stage of the cycle. Quantification of mRNA levels of **(B)** *Nlrp3*, caspase-1 (*Casp1*), interleukin-1b (*Il-1*b), and interleukin-18 (*Il-18*) by real-time PCR. Abundance of **(C)** NLRP3, **(D)** pro CASP1 p45, **(E)** CASP1 p20, **(F)** pro IL-18 p24, and **(G)** IL-18 p18 protein during **(E,D)** measured by Western blotting analysis. Data were normalized to ribosomal protein L37 (*Rpl37*) mRNA expression and b-actin of or glyceraldehyde 3-phosphate dehydrogenase (GAPDH) protein expression. Bars represent mean SEM. Statistical analysis between groups was carried out using Mann–Whitney. Number of samples: $n = 6–7$ for real-time PCR analysis and $n = 7–8$ immunoblots. Asterisks indicate significant differences ($p < 0.05$; $p < 0.01$). Representative immunohistochemistry (IHC) staining ($n = 2–3$) of NLRP3 protein during follicular development in the mouse ovary. Positive staining in brown, counterstaining with hematoxylin. **(H,J)** Negative control incubated with secondary antibody. Localization of NLRP3 in **(I)** whole ovary of 16 weeks (wk) mice fed chow diet (CD), **(K)** primary follicles of 16- week CD mice, **(L)** secondary follicles of 16- week high-fat diet (HFD) mice, and **(M)** preantral follicles of 16- week CD mice. Staining was detected in granulosa (GC) and theca (TC) cells (TC). Faint18 7 Tf 5.964 0 Td [eEgge5og68(Ah((HFD Td [(sgv50TC).)-278-l051.)-278gsgv50TC).)-2778(durin-278eting)-278(Ar)-278(itaining)-nosks iheadtaining),anoblots.

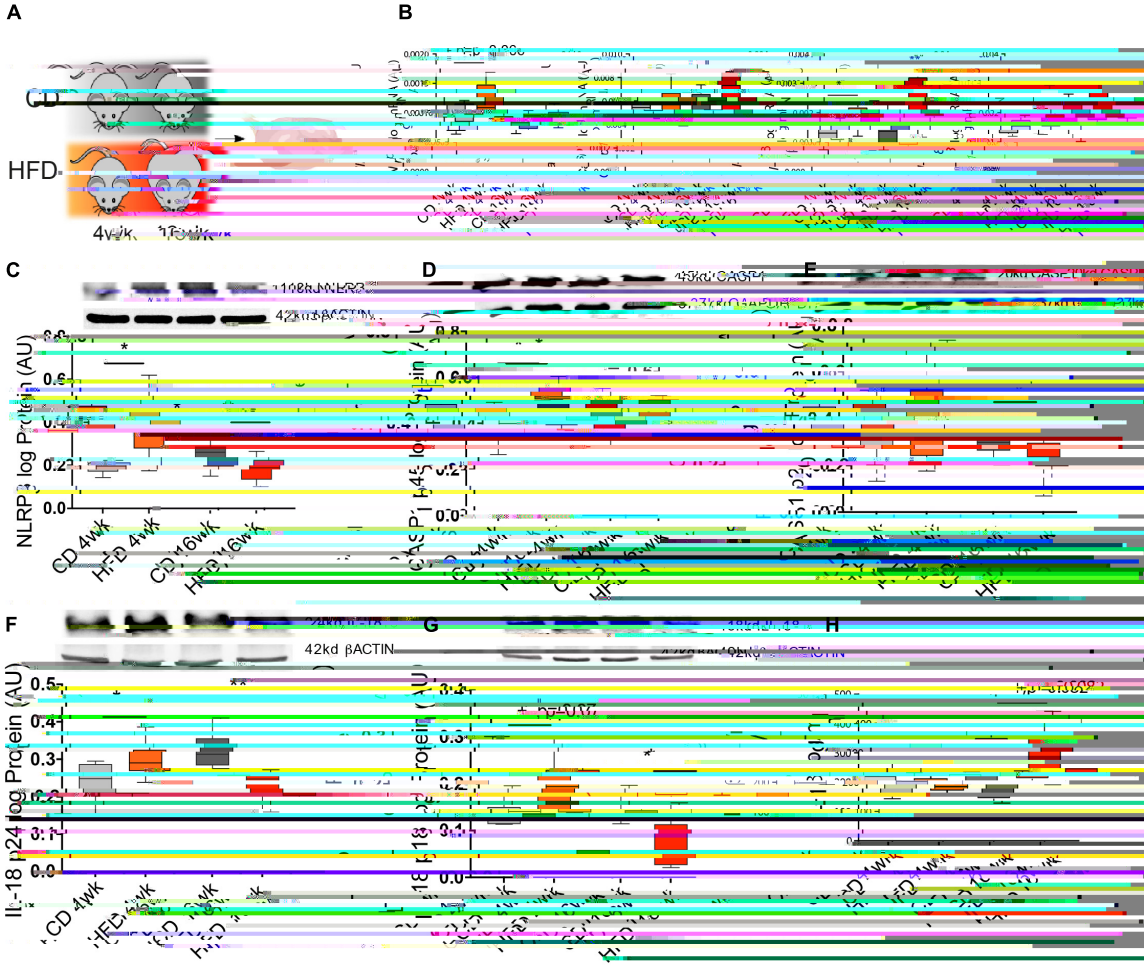

FIGURE 2 | Diet-induced obesity (DIO) changes NLRP3 expression in the ovary. **(A)** Experimental design: Mice were fed either chow diet (CD) or high-fat diet (HFD) for 4 or 16 weeks (wk) and ovaries were collected during the diestrus stage. Quantification of **(B)** *Nlrp3*, *Casp1*, *Il-1*b, and *Il-18* mRNA by real-time PCR. Abundance of **(C)** NLRP3, **(D)** pro CASP1 p45, **(E)** CASP1 p20, **(F)** pro IL-18 p24, **(G)**

TABLE 3 | Body weight measurement of three mouse models.

	0 week	4 week	8 week	12 week	16 week
CD	17.0 (0.6) g	19.7 (1.0) g	20.0 (0.9) g	20.9 (1.0) g	22.6 (2.5) g
HFD	19.4 (0.8) g	24.8 (2.5) g****	29.1 (3.6) g****	33.1 (4.3) g****	37.6 (3.7) g****
	0 day	**3 days**	**9 days**	**12 days**	**16 days**
C	21.7 (1.7) g	22.8 (2.0) g	22.1 (2.1) g	21.5 (1.6) g	21.9 (1.9) g
L	21.8 (1.9) g	20.5 (1.9) g	19.0 (1.4) g**	18.5 (1.2) g***	19.4 (1.7) g
	8 week	**9 week**	**10 week**	**11 week**	**12 week**
ob/ob C/?	20.9 (1.6) g	21.5 (1.6) g	22.2 (1.6) g	22.8 (2.1) g	22.7 (2.1) g
ob/ob –/–	39.8 (5.4) g****	43.1 (5.0) g****	45.0 (4.7) g****	47.4 (5.7)****	48.8 (4.0) g****

*DIO, Diet-induced obese; CD, mice were fed chow diet; HFD, high-fat diet (ii) pharmacologically hyperleptinemic mice were treated with saline (C) or leptin (L) for 16 days; (iii) genetically obese mice lacking leptin (ob/ob /) and control group (ob/ob C/?). Values presented in grams (g) of body weight and measurements made after weeks (wk) or days (d) within the specific protocol. Statistical analysis between groups was carried out using simple t-test. Asterisks indicate significant differences (**p < 0.01; ***p < 0.001; ****p < 0.0001).*

periodically (**Table 3**). Ovaries from all groups were collected and processed for mRNA and protein expression analysis. Real-time PCR analysis (n = 6–8/group) revealed an increase in *Nlrp3* and *Casp1* in 16 L, but a decrease in *ob/ob / * mice (**Figure 3B**, $p < 0.05$). Furthermore, the mRNA of *Il-1*b was upregulated in 16 L (**Figure 3B**, $p < 0.05$). Finally, the mRNA of *Il-18* was significantly downregulated in the *ob/ob / * group (**Figure 3B**, $p < 0.05$). With regard to protein expression (n = 6–8/group), we found that the 16 L group presented increased levels of NLRP3 (**Figure 3C**, $p < 0.05$), whereas the opposite pattern was observed in *ob/ob / * mice, compared with control groups (**Figure 3C**, $p < 0.05$). Accordingly, both pro-peptides CASP1 (p45) and CASP1 (p20) showed increased levels in 16 L (**Figures 3D,E**; $p = 0.07$ and $p < 0.05$, respectively); nonetheless, no significant changes were found in the *ob/ob* model. Importantly, IL-1b protein levels measured by ELISA (n = 4–5/group) were increased in 16 L, but decreased in *ob/ob / * (**Figure 3F**, $p < 0.05$). In this experiment, we revealed the functional link between leptin signaling and NLRP3 inflammasome component regulation in the ovary, with leptin treatment inducing the activation of NLRP3 and CASP1 with subsequent secretion of IL-1b. Furthermore, we confirmed the downregulation of NLRP3 expression in the ovaries of *ob/ob / * .

Leptin Promotes Changes of NOD-Like Receptor Protein 3 Inflammasome Components Gene Expression in Cumulus Cells During Early Onset of Obesity

In this experiment, we examined whether the association between leptin signaling and NLRP3 inflammasome activation previously observed in whole ovaries holds true at the cellular level. We, therefore, analyzed particularly the somatic companions of the female gamete, the CCs. We started reanalyzing the RNA sequencing (RNA-seq) datasets from CCs from 4- and 16-week DIO and pharmacological hyperleptinemic model (**Figure 4A**; Wołodko et al., 2020). We confirmed the expression levels of leptin and NLRP3 pathway components for 16 L and 4-week HFD, and despite no changes in *Nlrp3* in CCs after 4-week HFD, the gene was upregulated in 16 L (**Figure 4B**). The low coverage of the samples (an average of 5.5 million reads) and the weak expression level of *Nlrp3* in CCs may account for the lack of changes in 4-week HFD. Nonetheless, the consistent upregulation of various components of the NLRP3 inflammasome, like *Nlrp3*, *Il-18*, *Casp1*, *Il-1*b, and *Asc* in 16 L is suggestive of the stimulatory e□ects of leptin on the expression level and activation of NLRP3 inflammasome genes also in CCs (**Figure 4B**). As previously shown, the DESeq analysis of 4-week DIO protocol revealed 997 di□erentially expressed genes (DEGs) in 4-week HFD, whereas for pharmacological hyperleptinemic model, a total of 2,026 DEGs were found in 16 L (Wołodko et al., 2020), in comparison with their control groups ($p < 0.05$; Wołodko et al., 2020). In the present analysis, we overlapped the DEGs from 4-week HFD and 16 L and identified seven genes either up- or downregulated in both conditions (**Figure 4C**). Subsequently, we integrated the 14 DEGs with the main components of NLRP3 and leptin signaling pathways (Wołodko et al., 2020), based on the correlation between their expression levels ($p > 0.90$), and obtaining five clusters (**Figure 4D**). Of note, one of the clusters revealed the gene interaction between *Casp1, phosphatase and tensin homolog (Pten)* and *signal transducer and activator of transcription 5a (Stat5a)*, while others showed a link between *Socs3* and *Il-1*b, known as an important axis involved in the mediation of immune response (Chaves de Souza et al., 2013). Importantly, other genes were highlighted in the network, as *solute carrier family 22 member 15 (Slc22a15)*, a cell membrane transporter and metabolic gene (Nigam, 2018), or *stress-associated endoplasmic reticulum protein 1 (Serp1)* involved in protein unfolding and stress response (Yamaguchi et al., 1999). Indeed, metabolic performance in the preovulatory follicle is tightly regulated and involves the crosstalk between GC and oocyte (**Figure 4D**; Wołodko et al., 2021). The gene ontology analysis for the presented network revealed three main events: negative regulation of glucose transport, positive regulation of cytokine biosynthesis, and response to ATP (**Figure 4E**, $p < 0.05$). Finally, we plotted a subset of [illegible]

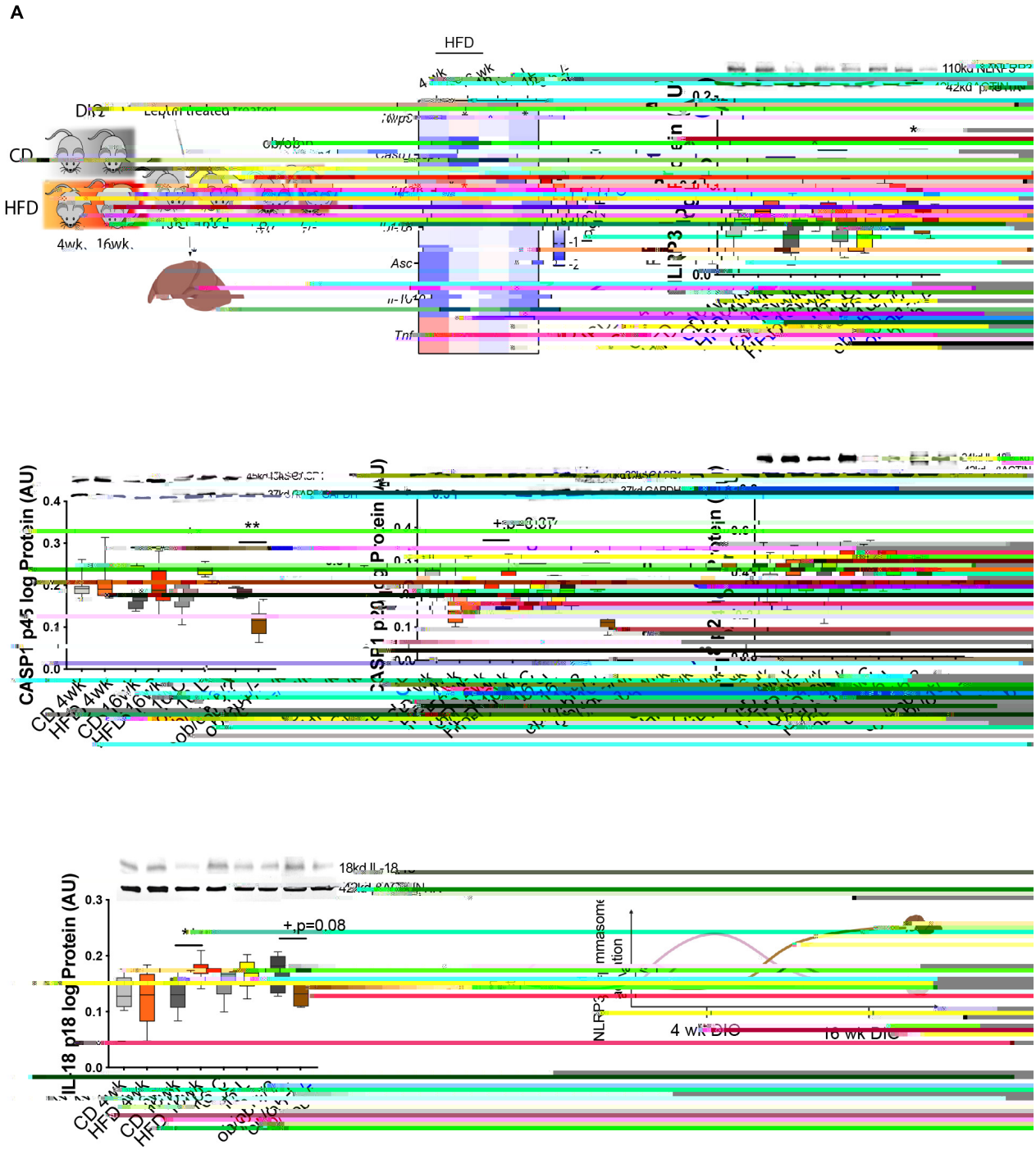
A
HFD
CD
HFD
4wk, 16wk
Asc
Tnf
CASP1 p45 log Protein (AU)
CD 4wk
HFD 4wk
CD 16wk
HFD 16wk
+,p=0.08
4 wk DIO
16 wk DIO

FIGURE 5 |

the proinflammatory mediators like *Il-1*b, *Il-6*, and *Tnf*a in the ovaries of mice fed HFD for 24 week (Nteeba et al., 2013). Hence, our results suggest the existence of alternative pathways to NLRP3 inflammasome mediating IL-1b upregulation in mouse ovaries at 16- week HFD (Schmidt and Lenz, 2012; Zhu and Kanneganti, 2017;

response (Robinson et al., 2016). On the contrary, the ovary is not only a highly immunogenic organ constantly secreting large amounts of cytokines and immune mediators (Piccinni et al., 2021) but also more prone to rapidly mount a proinflammatory response during obesity. Indeed, the inability of the ovary to control inflammation, and the exacerbated activation of cytokine production, certainly ascribes for the great vulnerability of the female gamete to maternal obesity even at earlier stages of disease progression. Thus, our results expose the increased vulnerability of the ovaries to maternal obesity, characterized by the development of an early inflammatory response that rapidly a□ects the gamete and impairs fertilization.

In summary, our work evidences the major role of leptin signaling on NLRP3 inflammasome activation in the ovary of mice during early obesity. Noteworthy, failure in ovarian leptin signaling in late obesity was associated with the repression in NLRP3 activity, but with maintenance of inflammation and levels of IL-1b. Moreover, NLRP3 inflammasome activation in the ovaries after early obesity contrasted with its activation exclusively during late obesity in the liver. Hence, the present findings suggest a greater vulnerability of the ovary, in general, and the gamete, in particular, to the energetic surplus during maternal obesity.

DATA AVAILABILITY STATEMENT

The data presented in the study are deposited in the Gene Expression Omnibus repository, accession number GSE180300.

ETHICS STATEMENT

The animal study was reviewed and approved by the Local Animal Care and Use Committee for University of Warmia and Mazury, Olsztyn. Guidelines for animal experiments followed EU Directive 2010/63/EU.

AUTHOR CONTRIBUTIONS

MA acquired, analyzed, interpreted the data, and wrote the manuscript. KW acquired, analyzed the data, revised, and edited the manuscript. JO performed the immunohistochemistry staining. JC-F conducted the data analysis and interpretation of data and revised the manuscript. DM performed the immunohistochemistry staining. GK revised and edited the manuscript. AG conceptualized and designed the study, acquired the funding, participated in the acquisition, analysis, interpretation of the data, and wrote and edited the manuscript. All authors contributed to the article and approved the submitted version.

FUNDING

This work was supported by grants from the Polish

Fu, S., Liu, L., Han, L., and Yu, Y. (2017). Leptin promotes IL-18 secretion by activating the NLRP3 inflammasome in RAW 264.7 cells. *Mol. Med. Rep.* 16, 9770–9776. doi: 10.3892/mmr.2017.7797

Galvão, A., Henriques, S., Pestka, D., Lukasik, K., Skarzynski, D., Maria Mateus, L., et al. (2012). Equine luteal function regulation may depend on the interaction between cytokines and vascular endothelial growth factor: an in vitro study. *Biol. Reprod.* 86:187. doi: 10.1095/biolreprod.111.097147

Galvão, A., Tramontano, A., Rebordão, M. R., Amaral, A., Bravo, P. P., Szóstek, A., et al. (2014). Opposing roles of leptin and ghrelin in the equine Corpus luteum regulation: an in vitro study. *Mediators Inflamm.* 2014:e682193. doi: 10.1155/2014/682193

Guglielmo, A., Sabra, A., Elbery, M., Cerveira, M. M., Ghenov, F., Sunasee, R., et al. (2017). A mechanistic insight into curcumin modulation of the IL-1b secretion and NLRP3 S-glutathionylation induced by needle-like cationic cellulose nanocrystals in myeloid cells. *Chem. Biol. Interact.* 274, 1–12. doi: 10.1016/j.cbi.2017.06.028

Guo, Q.-J., Shan, J., Xu, Y.-F., Hu, Y.-Y., Huo, C.-L., Song, J.-Y., et al. (2020). Pioglitazone metformin complex improves polycystic ovary syndrome comorbid psychological distress via inhibiting NLRP3 inflammasome activation: a prospective clinical study. *Mediators Inflamm.* 2020:3050487. doi: 10.1155/2020/3050487

Gurung, P., Anand, P. K., Malireddi, R. K., Vande Walle, L., Van Opdenbosch, N., Dillon, C. P., et al. (2014). FADD and caspase-8 mediate priming and activation of the canonical and noncanonical NIrp3 inflammasomes. *J. Immunol. (Baltimore, Md. 1950)* 192, 1835–1846. doi: 10.4049/jimmunol.1302839

Hasegawa, A., Mochida, K., Inoue, H., Noda, Y., Endo, T., Watanabe, G., et al. (2016). High-Yield superovulation in adult mice by anti-inhibin serum treatment combined with estrous cycle synchronization. *Biol. Reprod.* 94:21. doi: 10.1095/biolreprod.115.134023

He, D., Liu, L., Wang, Y., and Sheng, M. (2020). A novel genes signature associated with the progression of polycystic ovary syndrome. *Pathol. Oncol. Res. POR* 26, 575–582. doi: 10.1007/s12253-019-00676-3

He, Y., Zeng, M. Y., Yang, D., Motro, B., and Núñez, G. (2016b). NEK7 is an essential mediator of NLRP3 activation downstream of potassium e□ux.

Odegaard, J. I., and Chawla, A. (2008). Mechanisms of macrophage activation in obesity-induced insulin resistance. *Nat. Clin. Pract. Endocrinol. Metab.* 4, 619–626. doi: 10.1038/ncpendmet0976

Palazón-Riquelme, P., Worboys, J. D., Green, J., Valera, A., Martín-Sánchez,